Application of TiO$_2$ photocatalytic oxidation and non-woven membrane filtration hybrid system for degradation of 4-chlorophenol

Ren-Yang Horng[a,b], Chihpin Huang[a*], Min-Chao Chang[b], Hsin Shao[b],
Be-Lain Shiau[b], Yen-Jung Hu[c]

[a]*Institute of Environmental Engineering, National Chiao Tung University, Hsinchu, Taiwan*
Tel. +886 (3) 572-6463; Fax: +886 (3) 572-5958; email: cphuang@mail.nctu.edu.tw
[b]*Energy and Environment Research Laboratories, Industrial Technology Research Institute, Hsinchu, Taiwan*
[c]*KNH Enterprise Co., Ltd., Taipei, Taiwan*

Abstract

A system coupling photocatalytic oxidation of titanium dioxide particles separated by non-woven membrane for the degradation of 4-chlorophenol in an aqueous solution was studied. Non-woven membranes with three different pore sizes were applied to compare their specific flux and permeate turbidity. The results showed that when the pore size was slightly smaller than secondary particles of photocatalyst, higher specific flux and lower turbidity permeate were obtained. Four different applied fluxes, 0.25, 0.5, 1.0 and 2.0 m^3/m^2/d, were used with a 2.0 µm pore size non-woven membrane in a continuous system. The results revealed that the transmembrane pressure (TMP) was less than 10 kPa in all applied fluxes, due to the formation of a porous dynamic cake layer on the surface of the membrane. Based on the filtration characteristics of non-woven membranes, we found that cake formation, rather than pore blocking or pore narrowing, was the dominant factor. This phenomenon also resulted in permeate turbidity ranging from 0.5 to 1.5 NTU and non-detectable concentration of TiO$_2$ in the permeate. At the same time the experimental results indicated that the concentrations of TOC and 4-chlorophenol decreased with decreasing applied flux, and that the concentration of chloride ions increased with decreasing applied flux in a 4-chlorophenol photodegradation test. It showed that 4-chlorophenol could be effectively degraded by this hybrid system with lower TMP and stable applied flux.

Keywords: Non-woven membrane; 4-chlorophenol; TMP; Flux; Photocatalytic

1. Introduction

In the past three decades, heterogeneous photocatalytic processes have been considered as one of the most promising advanced oxidation processes (AOP) for water and wastewater treatment containing refractory organic pollutants. This technology can be applied in two different ways, i.e. suspended and fixed type. The suspended photocatalyst has a more effective

*Corresponding author.

photocatalytic activity than the fixed type due to having many active surface sites. However, the effective separation of suspended photocatalysts from aqueous solution is still an issue. In recent years, the separation of the photocatalysts from the liquid phase has been tried by using MF [1], UF [2] or even NF [3] membranes. However, problems such as low flux, high operational pressure and membrane fouling have not been overcome yet.

It is well known that non-woven fabric material with random structures is cheaper and has extensive application as a filter material for water treatment [4]. In our laboratory, the successful application of submerged non-woven fabric membrane bioreactor technology for industrial wastewater treatment [5] and wasted sludge reduction [6] has been developed. Meanwhile, a side stream of non-woven membrane to separate photocatalysts has been established in our laboratory for the degradation of methylene blue [7]. A hybrid system combining photocatalytic oxidation by titanium dioxide with particles separated by a submerged non-woven membrane was also studied. Hence the aim of this study was to investigate the performance and filtration characteristics of membrane fouling of hybrid systems with various applied fluxes, and the subsequent photodegradation of 4-chlorophenol (4-CP) as a model compound in water.

2. Methods and materials

2.1. Membranes, TiO$_2$ and 4-chlorophenol characteristics

Three different non-woven membranes, A, B and C, with pore sizes of 0.2, 2.0, and 20.0 μm, respectively, manufactured by KNH, Taiwan, were used in a batch study. Nominal pore sizes of the membranes were determined by air bubble method (Automated perm porometer, Porous Materials, U.S.A.). Total area of each membrane was 0.02 m^2 for both sides of membrane. A

spacer was installed inside the membrane to provide a conduit for the permeate. The membrane's support layer was made of polyester. In the continuous system, membrane B was selected with total surface area of 0.045 m^2 for both sides.

Degussa P25 TiO$_2$ powder with a primary particle size of 20–30 nm was selected. Average aggregated secondary particle size after aggregation in the liquid phase was measured by a zeta potential analyzer (Zetaplus, Brookhaven Instruments, USA) and ranged from 3 to 8 μm, depending on different pH values and aeration intensities in the solution.

The residual turbidity of the permeate from different pore size membranes and applied fluxes was measured by turbidity meter (2100P Turbidimeter, Hach, USA). The 4-chlorophenol was analyzed by HPLC (Incelligent 500 and UV-2075 Incelligent UV/Vis detector), mobile phase (CH$_3$OH/H$_2$O=50 50, added 1% CH$_3$COOH), and Column: YMC-Pack Pro C$_{18}$ R.S. (150 mm× 4.6 mm, ID S-5 μm). The chloride ion was quantified by IC (ICS-90 chromatography system, Dionex). Organic carbon was detected by TOC (Liqui TOC, Eelementar).

2.2. Experimental operations and conditions

The schematic diagram of our non-woven membrane system used in this study is shown in Fig. 1. Our system consisted of a reactor in which the membrane module was submerged. Three reactors were installed in parallel and each rectangular tank had a working volume of 8 L. The membrane module containing two parts of non-woven membrane plate was made of polyester. The pore size of non-woven membrane tested was 0.2 μm (membrane A), 2.0 μm (membrane B) and 20.0 μm (membrane C), respectively. The effective filtration area was 0.02 m^2 for each flat membrane. The aeration units were installed at the bottom part of the reactor to maintain suspended particles in reactor, and also induce a cross flow along the membrane surface. The
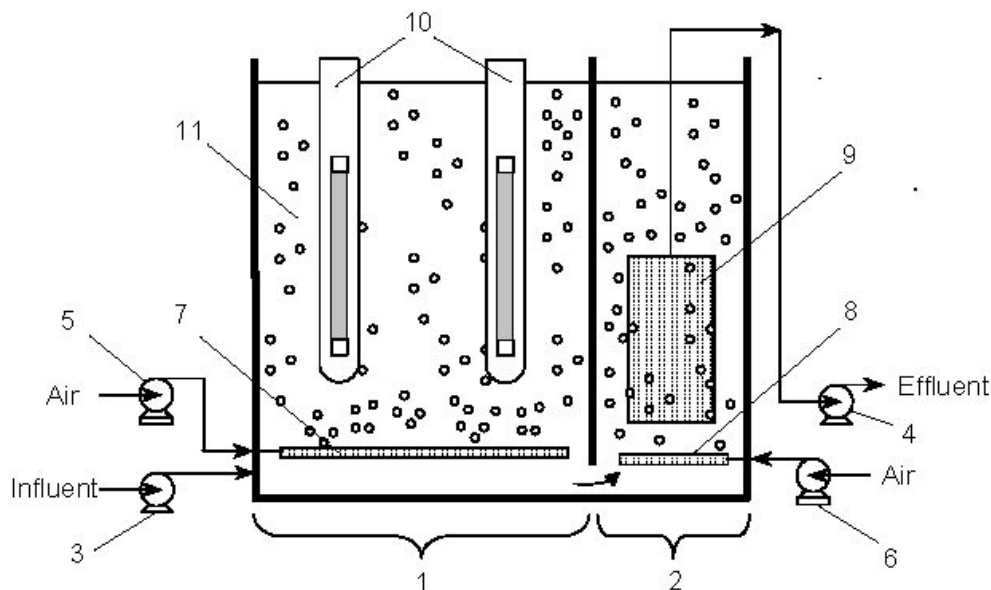
Fig. 1. Schematic diagram of the hybrid system coupling photocatalytic oxidation with a non-woven membrane reactor. 1 photocatalyticreaction region, 2 membrane separation zone, 3 influent pump, 4 effluent pump, 5 and 6 blower, 7 and 8 air distributor, 9 membrane module, 10 UVA lamp, 11 photocatalyst suspension.

permeate was drawn by a suction pump. A vacuum pressure gauge and flow meter were installed and connected to a computer to monitor transmembrane pressure (TMP) and record flow rate during the entire experiment.

In consecutive tests, the configuration of the treatment system was same as in the batch experiment, as shown in Fig. 1, but the volume of the reactor was different. The reactor was made of Pyrex glass with a working volume of 22.4 L. The reactor was divided into two sections by a UV light blocking baffle: a photocatalytic reaction region with volume of 16 L, and a membrane separation region with volume of 6.4 L. The non-woven fabric membrane module with membrane B was submerged in the membrane separation zone. In each experiment, aqueous suspensions of TiO_2 containing same amount of 4-chlorophenol were mixed by air and irradiated by UV light with different applied fluxes or pH values, as listed in Table 1. The UV radiation was performed by a set of four black lamps with 4 W or

Table 1
Operating conditions in the continuous system of coupling photocatalytic oxidation with non-woven membrane

Run no.	Operating conditions
1	Raw wastewater
2	Flux = 1.0 m/d, pH = 8.5, light =4 W
3	Flux = 1.0 m/d, pH = 6.5, light = 4 W
4	Flux = 1.0 m/d, pH = 4.5, light = 4 W
5	Flux = 1.0 m/d, pH = 6.5, ligh t =8 W
6	Flux = 0.25 m/d, pH = 6.5, light = 8 W
7	Flux = 0.5 m/d, pH = 6.5, light = 8 W
8	Flux = 2.0 m/d, pH = 6.5, light = 8 W

Same conditions for each run: TiO_2 conc. =2,000 mg/L, aeration intensity = 0.14 $m^3/m^2/min$

8 W power and wavelength of 365 nm. Light intensity of each lamp was 6 mW/cm^2. The 4-chlorophenol was of chemical reagent grade. All experiments including batch and continuous tests were performed at room temperature (25 °C).

2.3. Filtration resistance and specific flux

The filtration resistance and specific flux were calculated by the following equations:

$$J = \frac{\Delta P}{\mu \left(Rc + Rn + Rb + Rm \right)} \quad (1)$$

where ΔP is the TMP (Pa), μ is the viscosity of the permeate (Pa.s), J is the permeate flux ($m^3/m^2/s$), and Rc, Rn, Rb and Rm are cake resistance, pore narrowing resistance, pore blocking resistance and membrane resistance (m^{-1}), respectively, and

$$S = \frac{J}{\Delta P} \quad (2)$$

where S is the specific flux ($m^3/m^2/d/kPa$) defined by applied flux divided by TMP and related to membrane permeability, J is the permeate flux ($m^3/m^2/d$), and ΔP is the TMP (kPa).

2.4. Resistance determinations

Total resistance (Rt) in terms of membrane resistance (Rm), cake resistance (Rc), pore narrowing resistance (Rn) and pore blocking resistance (Rb) was measured in this study. Rc and Rn were considered as reversible fouling, and Rb was defined as irreversible fouling. Rm was determined using deionized (DI) water without TiO_2 particle for 8 h to record TMP and applied flux before suspended TiO_2 was filtrated. Rc was reversed by increasing aeration intensity to 5 NL/min for 2 h after the experiment had been completed and the porous dynamic cake layer had been formed. Once the cake had been removed, DI water was sucked through the system for 8 h before recording TMP and applied flux. For the Rn experiment, backwash using air from inside the non-woven membrane was conducted with an air flow rate of 5 NL/min for 2 h to remove par-ticles narrowed inside the membrane. Then DI water was used and sucked through the membranes for a further 8 h to record TMP and applied flux. Finally, Rb was calculated by the difference between Rt and the sum of Rc, Rn and Rm.

3. Results and discussion

3.1. Formation of a porous dynamic cake layer on non-woven membrane with good filtration capabilities

The SEM image of the virgin structure of a non-woven membrane created by random over-lapped fibers using the melt brown method is shown in Fig. 2(A). The pore size of the membrane was determined by size of fiber and fiber mass of filtering layer [8]. The porous dynamic cake layer formed on the membrane surface after filtration of TiO_2 particles from slurry with membrane B is shown in Fig. 2 (B). It was found that good filtration performance in terms of reduction of residual turbidity in permeate was observed, as depicted in Fig. 3. The residual turbidity was reduced from 100 to 1 NTU within 2 min, as depicted in the inset in Fig. 3. As for the applied flux, an initial applied flux of 6.0 $m^3/m^2/d$ was maintained during all experimental periods. It was also interesting to see that TMP accumulated slightly and finally became stable, as shown in Fig. 3. This result was different from that reported in the literature [9]. The dynamic layer formed on the membrane surface of UF or MF has also been proposed [9]. However, declining flux and accumulated TMP were usually observed in MF or UF systems, even if dynamic cake layers were formed. The reason was that the particles passing the non-woven membrane did not clog the pores before formation of the porous dynamic cake layer, due to the larger pore size of the non-woven membrane used. That is to say that less pore narrowing or pore blocking was observed for non-woven membranes with larger
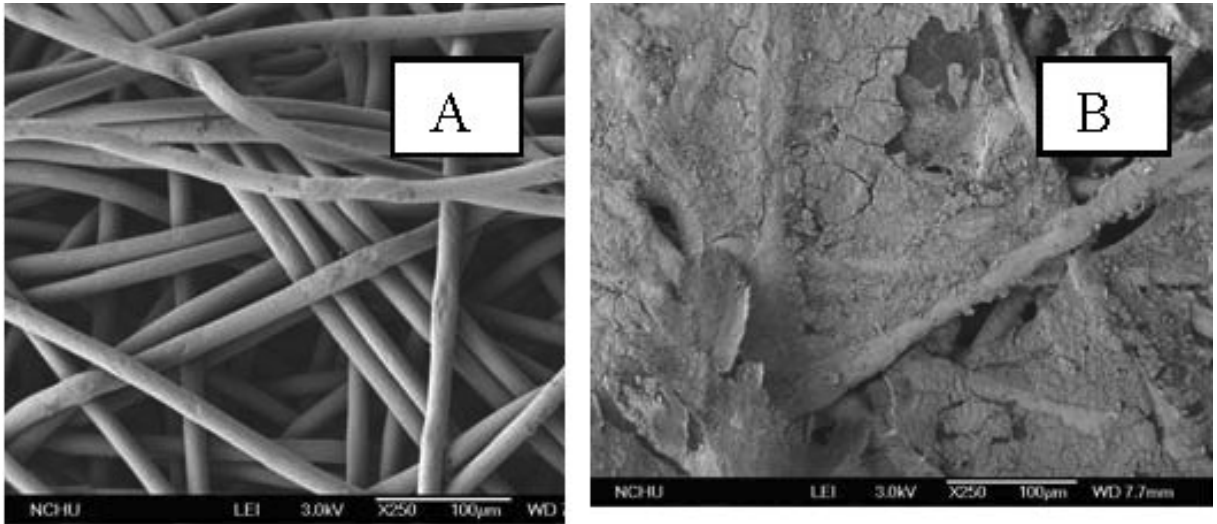
Fig. 2. SEM images for the surface of non-woven membrane before filtration (A) and after filtration (B).
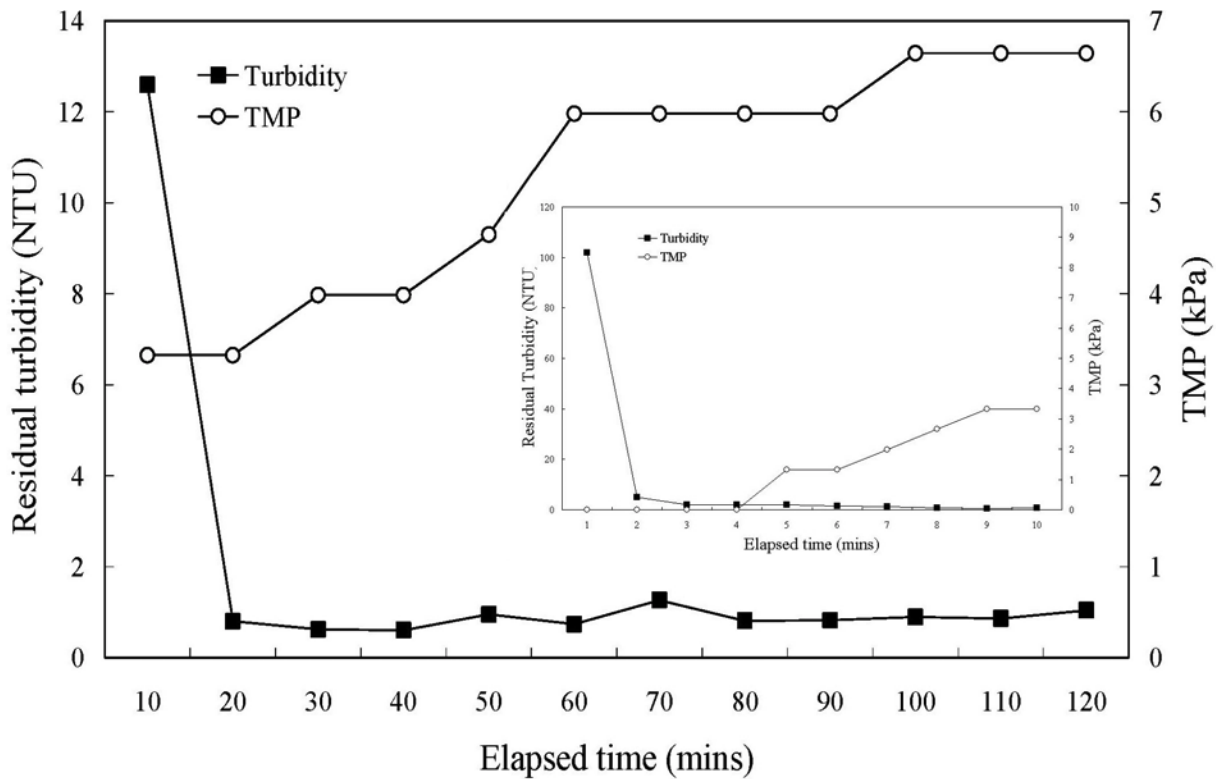

Fig. 3. Relationship between residual turbidity and TMP during formation of a porous dynamic cake layer (conc. of TiO_2 = 500 mg/L, flux = 6.0 $m^3/m^2/d$, aeration intensity = 8.4 $m^3/m^2/h$, pore size of non-woven membrane = 2.0 μm and pH 8.5).

pore sizes, comparing with that used in MF or UF systems. In fact, the non-woven membrane could be considered as a support layer in this case.

3.2. Relationship between pore size and particle size filtrated by non-woven membrane

Nano-scale primary particles of TiO_2, ranging from 20 to 30 nm, dispersed in an aqueous solution, were accumulated as secondary particles of several micro-scales [10]. To remove particle sizes bigger than 1 μm, non-woven fibrous materials are extensively used to provide the desired contaminant control [11]. In selecting appropriate pore sizes of non-woven membranes and controlling non-woven membrane fouling, it is necessary to consider the relationship of TMP and applied flux simultaneously. The calculated specific flux for three pore sizes of the non-woven membrane i.e. 0.2 μm, 2.0 μm, and 20 μm was 0.11, 0.50, and 0.53 $m^3/m^2/d/kPa$, respectively, under following experimental conditions: 1,000 $mgTiO_2/L$, pH 8.5, aeration intensity 8.4 $m^3/m^2/h$, and initial applied flux 3.0 $m^3/m^2/d$, as depicted in Fig. 4. It can be seen that the pore size of a non-woven membrane was critical in determining the specific flux. For smaller pore sizes, the specific flux dropped dramatically. This was due to the membrane becoming clogged by tiny particles before the establishment of cake filtration.

For practical applications, permeate water quality must also be considered. It was found that the quality of the permeate deteriorated when particle sizes were smaller than membrane pore sizes, as presented in Fig. 4. This resulted from the fact that the particles passed the membrane, producing higher residual turbidity in the permeate. Hence, the optimum non-woven membrane was one with a pore size slightly smaller than the size of the average secondary TiO_2 particles. Our experimental result differed from that of Molinari [12], who found lower specific flux in a system using photocatalysis coupled

with MF or UF membranes. However, in our system, higher specific flux could be obtained using non-woven membrane with an optimum pore size to separate μm range of accumulated TiO_2 particles

3.3. Fouling characteristics of the non-woven membrane in our system

The fouling characteristics in terms of cake formation, pore narrowing and pore blocking for three different pore sizes i.e. 0.2, 2.0 and 20.0 μm were examined under the following experimental conditions: TiO_2 =1,000 mg/L, air intensity = 8.4 $m^3/m^2/h$, pH=8.5 and initial flux=3.0 $m^3/m^2/d$. The results shown in Fig. 5 reveal that cake formation was the dominant factor and pore narrowing and pore blocking were only minor factors in the three different pore sizes of the membranes. The fact that maintained stable flux and quite low TMP in our experimental system, implied that the porous dynamic cake layer formed on the non-woven membrane surface, has excellent filtration ability for separation TiO_2 from slurry. However, we also found (Fig. 5) that the ratio of pore narrowing and pore blocking in smaller pore-sized membranes (0.2 and 2.0 μm) is greater than that of a larger pore-sized membrane (20.0 μm) because particles could be entrapped inside small pores of the membrane before a porous dynamic cake layer was formed. The clogging effect was more dominant for smaller pore-sized membranes. These results were different to MF membranes dominated by pore blocking [13]. Seminario et al [14] also mentioned that particle capture and size exclusion were considered the dominant mechanism of membrane fouling when MF membranes were used. The comparison between our non-woven system and traditional MF or UF systems found that filtration behavior was quite different. The larger pore sizes of non-woven membrane's supporting and porous dynamic cake layers dominated the filtration layer, resulting in a stable
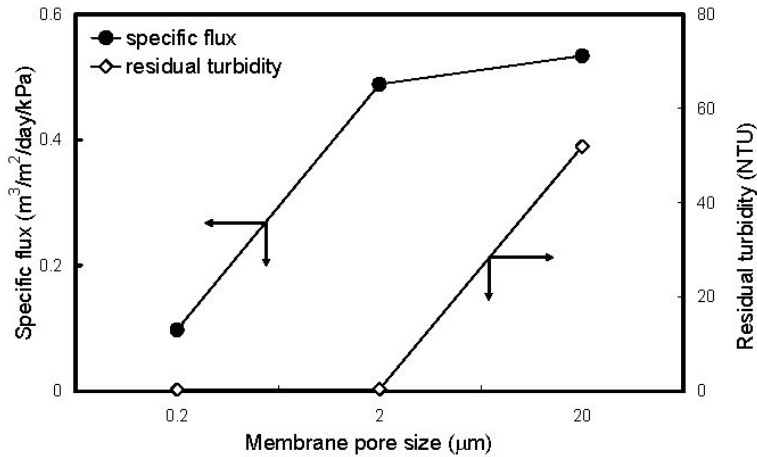
Fig. 4. Variation of specific flux and residual turbidity for three different pore sizes of membrane (TiO$_2$ conc.= 1,000 mg/L, aeration intensity = 8.4 m^3/m^2/h, and pH 8.5).
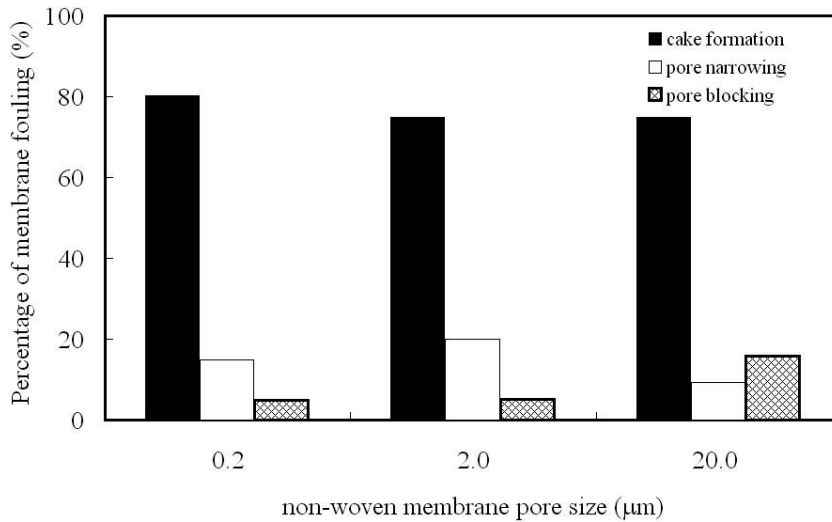

Fig. 5. Portion of cake formation/pore narrowing and pore blocking in the non-woven membranes with three different pore sizes. TiO$_2$ conc. =1,000 mg/L, air intensity= 8.4 m^3/m^2/h, pH 8.5, initial applied flux = 3.0 m^3/m^2/d.

applied flux and lower TMP. Meanwhile, intersection pores inside the non-woven membrane also provided many linking tunnels for fluid flow, even if some pores had become blocked [4].

3.4. Aeration intensity effect

Due to the larger pore sizes of non-woven membranes used, resistance from the membrane itself could be as low as zero. Thus, in our non-woven membrane system, resistances including cake formation, pore narrowing and pore blocking were the major contributor towards total filtration resistance. According to the pressure driven membrane filtration model [15], cake filtration resistance is proportional to the thickness of the cake layer, which was balanced by the force of adhesion and drag on the surface of the
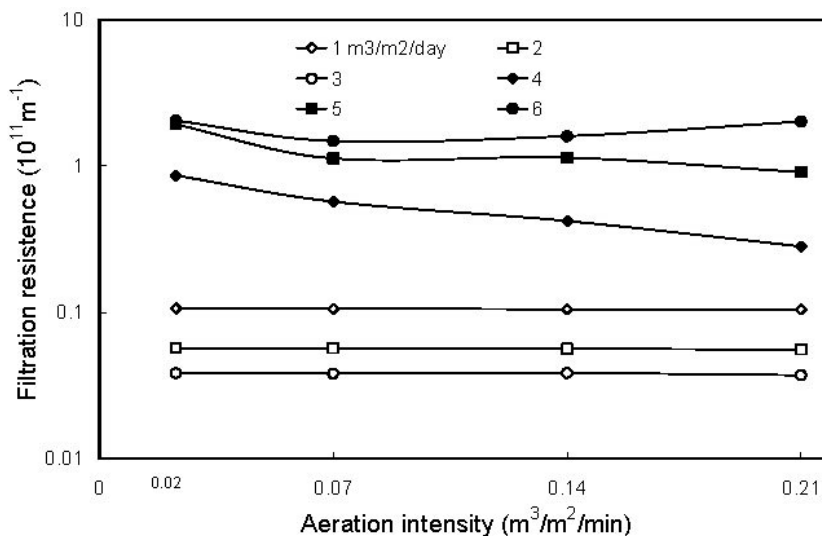
Fig. 6. Variation of filtration resistance with change of aeration intensities (TiO_2 conc. = 2,000 mg/L, membrane pore size = 2.0 μm, filtration time = 2 h, and pH 8.5).

membrane. The thickness of the cake layer on the membrane surface was related to crossflow velocity and applied flux. The variation of filtration resistance with different aeration intensities is shown in Fig. 6. It can be seen that the relationship between filtration resistance and aeration intensity showed no obvious change when the applied flux was 3.0 $m^3/m^2/d$ or less. Under these circumstances, a crossflow velocity along the membrane surface induced a shear stress, generating a back-transport balance, or re-entrainment of particles from the surface of the membrane [16]. However, when applied flux was higher than 3.0 $m^3/m^2/d$, the filtration resistance increased with decreasing aeration intensity. The reason was that the thickness of the cake layer accumulating on the non-woven membrane increased, and resulted in higher resistance at lower aeration intensities. On the other hand, filtration resistance also increased with aeration intensities that were too high at higher applied flux. In this instance a cake layer was incompletely formed and aggregated particles broke into smaller fragments with higher aeration

intensities [17], and titanium dioxide particles easily penetrated the membrane, resulting in higher filtration resistance.

3.5. TiO_2 concentration effect

In a suspension photocatalytic oxidation system, exceptionally high concentrations of TiO_2 are an obstacle to the adsorption of UV or UV-visible light, and result in a reduction of its efficiency [18]. The higher concentration of TiO_2, resulting in higher surface area, was expected to enhance the photocatalytic efficiency. Consequently we also looked into the concentration effect of TiO_2 on filtration behavior. The variation of filtration resistance with concentrations of TiO_2 using different applied fluxes is shown in Fig. 7. Nearly no filtration resistance was observed for all concentrations of TiO_2 when applied flux was 3.0 $m^3/m^2/d$. However, the filtration resistance increased by increasing the concentration of TiO_2 when the applied flux was 4 $m^3/m^2/d$ or more. Our results were different from that of Mozia et al. [1]. They found out that

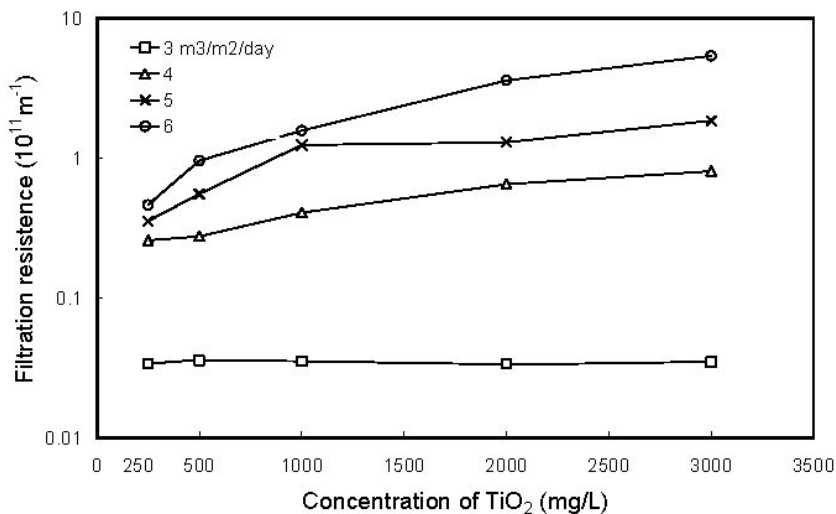Fig. 7. Variation of filtration resistance with different concentrations of TiO_2 (aeration intensity = 0.14 $m^3/m^2/min$, membrane pore size = 2.0 μm, filtration time = 2 h, and pH 8.5).

the concentration of photocatalyst, ranging from 100 to 500 mg/L, had no significant reverse effect However, Sopajaree et al. [19] revealed that the higher the concentration of photocatalyst, the lower the permeability obtained when concentrations of TiO_2 particles ranged from 500 to 3,000 mg/L, separated by an UF membrane. The major difference between microporous membranes and our non-woven membrane was pore size. The pore size of non-woven membranes used in this study was much larger than that of microporous membranes. Hence, the reason for achieving a stable permeate flux and lower TMP in a large pore-sized non-woven membrane reactor system at applied flux of 3 $m^3/m^2/d$ is due to the formation of a membrane-like, porous dynamic cake layer on the non-woven membrane surface [7]. The thickness of this porous dynamic cake layer was maintained, and resulted in a constant filtration resistance when aeration intensity was set at 0.14 $m^3/m^2/min$. As applied flux increased, the imbalance between adhesion and drag forces on the surface membrane occurred. The greater the concentration of photocatalyst, the greater the thickness of the cake layer that

was formed, resulted in higher filtration resistance.

3.6. Long-term system performance for photo-degradation

3.6.1. Variation of 4-chlorophenol concentration

The concentration of 4-CP in different test runs with operating conditions listed Table 1 is shown in Fig. 8. The initial concentration of 4-CP was 28.8 mg/L in run 1. Different removal efficiencies were obtained for different operating conditions. Lower concentrations of 4-CP in permeate was observed for lower pH value, shown in runs 2, 3 and 4. It can also be seen that concentrations of 4-CP decreased with the increase in light intensity, in comparing the data of run 3 and 5. The concentrations of 4-CP at different fluxes i.e. 0.25, 0.5, 1.0 and 2.0 $m^3/m^2/d$ are shown in runs 6, 7, 5, and 8. It can be seen that the concentration of 4-CP in permeate was proportioned to increasing applied fluxes, due to shorter reaction time. More than 92% of 4-CP removal was observed in run 6. The trend of 4-CP concen-
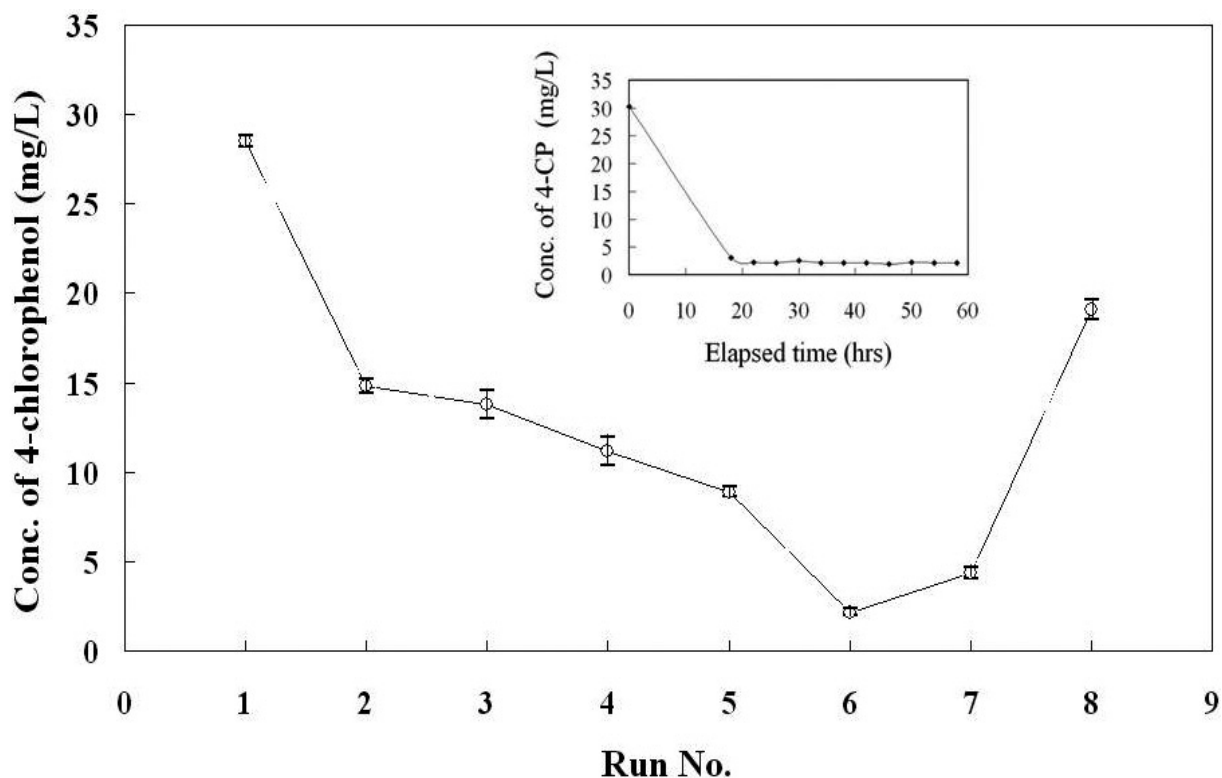
Fig. 8. Concentration of 4-chlorophenol in a hybrid system for different test runs.

tration in permeate, after photodegradation, during longer experimental periods, is also shown in the inset in Fig. 8. The experimental results indicated that removal efficiency could be fairly stably maintained in run 7, and no harmful effect, such as inactivation of the photocatalysts, was observed in our system, when 4-CP was degraded in consecutive operating modes.

3.6.2. Variation of TOC concentration

The variation of TOC is depicted in Fig. 9. The trend of TOC change was coincident with that in 4-CP shown in Fig. 8. However, the removal efficiency was different, as summarized in Table 2. TOC removal efficiency was between 10 and 20% lower than that in 4-CP, because 4-CP was transformed to other intermediate

Table 2
Removal efficiency of 4-CP and TOC in the hybrid system

Run No.	2	3	4	5	6	7	8
4-CP (%)	48	52	61	69	92	85	33
TOC (%)	27	31	52	51	81	65	20

products, e.g. hydroquinone and hydroxyhydroquinone [20], rather than carbon dioxide formed by complete oxidation.

3.6.3. Formation of chloride ion

4-CP was degraded by the photocatalytic system to produce intermediate or final products, and release chloride ions simultaneously in the presence of dissolved oxygen [20]. The variation
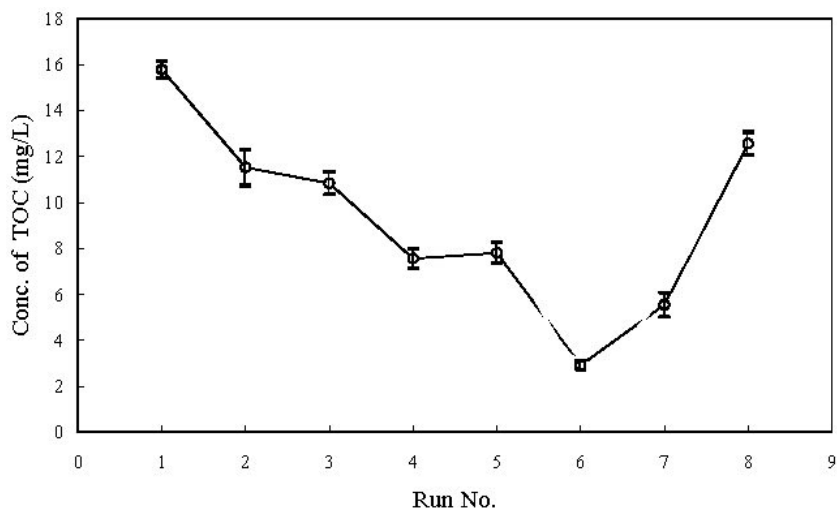
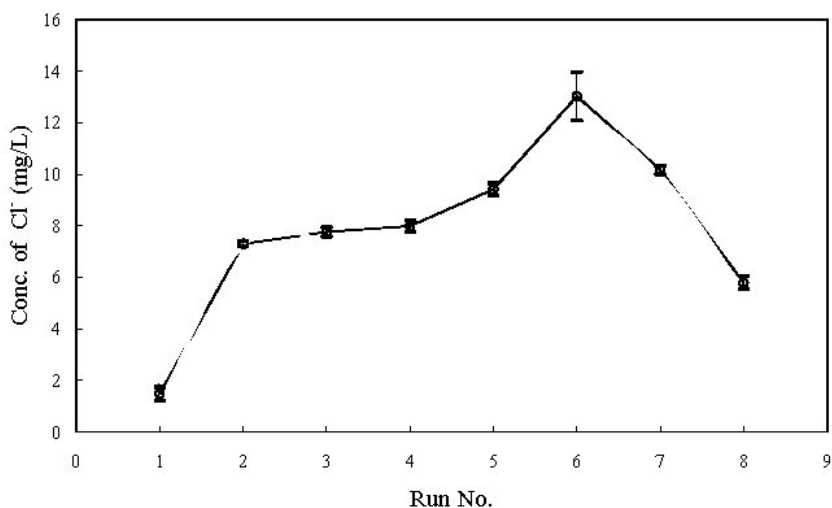Fig. 9. Concentration of TOC in a hybrid system for different test runs.

Fig. 10. Chloride concentration in the permeate for different test runs.

of chloride ion concentration in the permeate (shown in Fig. 10 in different test runs) was evidence of photodegradation of 4-CP. As can be seen in this figure, the formation of chloride ions matched the degradation degree of 4-CP. The highest concentration of chloride ion was 13 mg/L in run 6 when the photodegradation efficiency of 4-CP was also the highest. The formation of chloride ions has an inhibitory effect on photocatalytic systems due to its competition with molecular oxygen for electron scavengers competing with molecular [21]. This inhibits the formation of superoxide radicals from the actual oxidation agent, resulting in a decrease of photocatalytic efficiency [22] Contrarily, in our consecutive hybrid system no significant side-
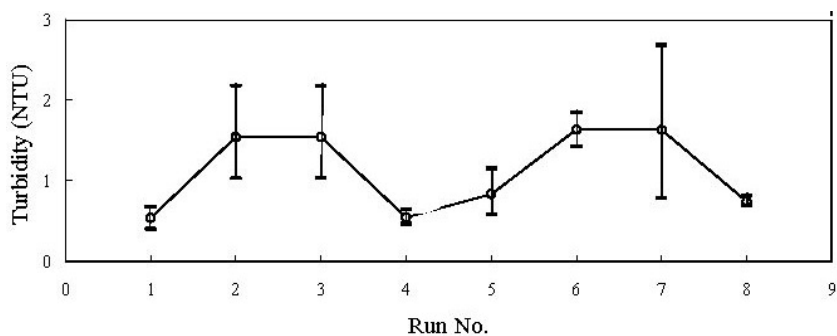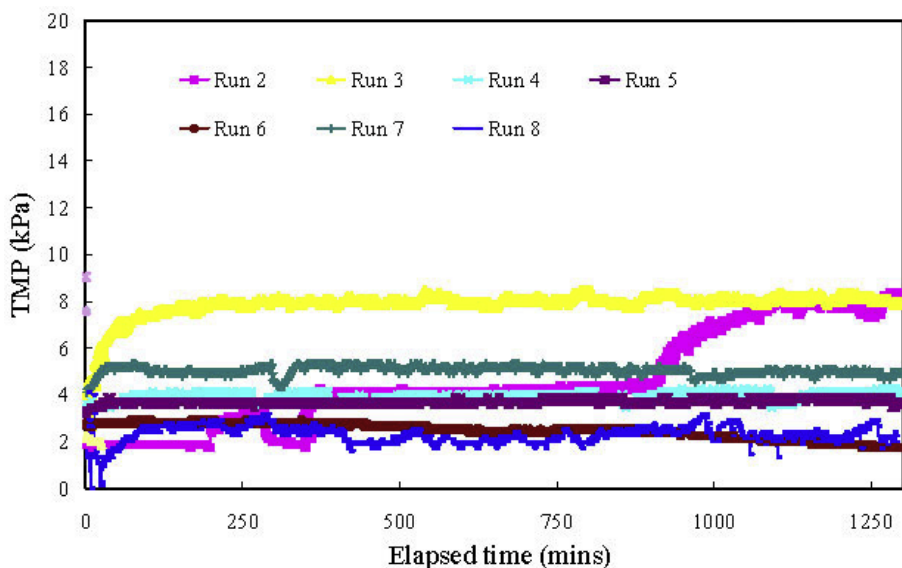
Fig. 11. Permeate turbidity for different test runs.

Fig. 12. Varaition of TMP in hybrid system for different test runs.

effects were observed in any of the test runs because the molecular oxygen supply was sufficient to induce a crossflow on the surface of non-woven membrane, unlimiting the formation of free radicals for the degradation of 4-CP.

3.6.4. Residual turbidity in the permeate

The pore size used in the non-woven membrane was larger than that used in MF or UF. In the early stages, some secondary particle photocatalysts passed through the non-woven membrane before the porous dynamic cake layer was formed. Photocatalysts in permeate that passed through the membrane not only reduced the concentration of photocatalysts in the reactor, but also deteriorated the water quality, e.g. generating higher turbidity in the permeate. The residual turbidity in terms of the photocatalyst's concentration was of concern and was measured in all experiments, as shown in Fig. 11. The permeate was in fact clear and contained only nondetectable concentrations of suspended solids (SS). Residual turbidity ranged from 0.5 to 1.5 NTU in the permeate. These results were similar to permeate produced from MF [23] or UF [1] for the separation of photocatalysts from liquid

solutions. The reason was that the porous dynamic cake layer formed on the surface of the non-woven membrane played a key role in obtaining the same water quality as MF or UF systems.

3.6.5. Variation of TMP

Filtration behavior dominated by cake formation on non-woven membranes to separate TiO_2 particles from slurry had a lower TMP. The variation of TMP in different test runs is as shown in Fig. 12. The TMP was less than 10 kPa even when different applied fluxes were used, with appropriate aeration intensity and without an extra backwash during long-term operation periods. The accumulated TMP in membrane systems was an indicator of potential membrane fouling [24]. TMP observed in our non-woven membrane system was usually lower than that of MF or UF, using separation photocatalysts from slurry. Therefore, a periodic back-wash was needed in the latter system to obtain long term stability conditions [25], or the fabrication of nano-structured TiO2/silica gel to avoid flux decline [26] has been proposed. However, a complicated mode of operation and additional costs attended these novel concepts and limited their practical application.

4. Conclusions

A hybrid system coupling non-woven membrane separation with photocatalytic oxidation process was conducted to obtain satisfied removal efficiency of a model compound with slight flux reduction and lower TMP accumulation. Cake formation on non-woven membranes was considered a key dominant factor, resulting in the formation of a porous dynamic cake layer on the surface of non-woven membrane for separation TiO_2 particles from slurry. This phenomenon also resulted in lower TMP and stable applied fluxes.

References

[1] S. Mozia, M. Tomaszewska, and A.W. Morawski, A new photocatalytic membrane reactor (PMR) for removal of azo-dye acid red 18 from water, Appl. Cataly. B: Environ., 59 (2005) 131–137.

[2] A.A. Lee, K.H. Choo, C.H. Lee, H.I. Lee, T. Hyeon, W. Choi and H.H. Kwon, Use of ultrafiltration membranes for the separation of TiO_2 photocatalysts in drinking water treatment, Ind. Eng. Chem. Res., 40 (2001) 1712–1719.

[3] R. Molinari, F. Pirillo, V. Loddo and L. Palmisano, Heterogeneous photocatalytic degradation of pharmaceuticals in water by using polycrystalline TiO_2 and a nanofiltration membrane reactor, Catalysis Today, 118 (2006) 205–213.

[4] A.F. Turbak, Non-woven: Theory, Process, Performance, and Testing. Tappi Press, Atlanta, GA, 1993.

[5] M.C. Chang, R.Y. Horng, H. Shao and Y.J. Hu, Performance and filtration characteristics of on-woven membranes used in submerged membrane bioreactor for synthetic wastewater treatment, Desalination, 191 (2006) 8–15.

[6] R.Y. Horng, H. Shao, W.K. Chang and M.C. Chang, The feasibility study of using non-woven MBR for reduction of hydrolyzed biosolids, Water Sci. Technol., 54(5) (2006) 85–90.

[7] M.C. Chang, R.Y. Horng, H. Shao and Y.J. Hu, Separation of titanium dioxide from photocatalytically treated water by non-woven fabric membrane. Filtration, 6(4) (2006) 340–344.

[8] D. Li, M.W. Fresy and Y.L. Joo, Characterization of nanofibrous membranes with capillary flow porometry, J. Membr. Sci., 286 (2006) 104–114.

[9] M.H. Al-Malack and G.K. Anderson, Formation of dynamic membranes with crossflow microfiltration, J. Membr. Sci., 112 (1996) 287–296.

[10] K.A. Guzman, M.P. Finnegan and J.F. Banfield, Influence of surface potential on aggregation and transport of titania nanoparticles, Environ. Sci. Technol., 40 (2006) 7688–7693.

[11] J.A. Destephen and K.J. Choi, Modeling of filtration processes of fibrous filter media, Sep. Technol., 6 (1996) 55–67.

[12] R. Molinari, M. Mungari, E. Drioli, A. Di Paola, V. Loddo, L. Palisano and M. Schiavello, Study on a photocatalytic membrane reactor for water purification, Catalysis Today, 55 (2000) 71–78.

[13] E. Iritani, Y. Mukai, M. Furuta, T. Kawakami and N. Katagiri, Blocking resistance of membrane during cake filtration of dilute suspensions, AIChE J., 51(9) (2005) 2609–2614.

[14] L. Semiario, R. Rozas, R. Borquez and P.G. Toledo, Pore blocking and permeability reduction in cross-flow microfiltration, J. Membr. Sci., 209 (2002) 121–142.

[15] S. Hong, P. Krishna, C. Hobbs, D. Kim and J. Cho, Variation in backwash efficiency during colloidal filtration of hollow-fiber microfiltration membranes, Desalination, 173 (2005) 257–268.

[16] T. Ueda, K. Hata, T. Kikuaka and O. Seino, Effects of aeration on suction pressure in a submerged membrane bioreactor, Water Res., 31(3) (1997) 489–494.

[17] C. Wisniewaki, A. Grasmick and A.L. Cruz, Critical particles size in membrane bioreactor case of a denifying bacterial suspension, J. Membr. Sci., 197 (2000) 141–150.

[18] M. Muruganandham and M. Swaminathan, Solar photocatalytic degradation of a reactive azo dye in TiO_2-suspension, Solar Energy Mat. Solar Cells, 81(4) (2004) 439–457.

[19] K. Sopajaree, S.A. Qasim, S. Basal and K. Rajeshwar, An integrated flow reactor-membrane filtration system for heterogeneous photocatalysis. Part II. Experiments on the ultrafiltration unit and combined operation, J. Appl. Electrochem., 29 (1999) 1111–1118.

[20] M. Moonsiri, P. Rangsunvigit, S. Chavadej and E. Gulari, Effects of Pt and Ag on the photocatalytic degradation of 4-chlorophenol and its by-products, Chem. Eng. J., 97 (2004) 241–248.

[21] J.M. Tseng and C.P. Huang, Removal of chlorophenols from water by photocatalytic oxidation, Water Sci. Technol., 23 (1991) 377–387.

[22] G. Alhakimi, S. Gebril and L.H. Studnicki, Comparative photocatalytic degradation using natural and artificial UV-light of 4-chlorophenol as a representative compound in refinery wastewater, J. Photochem. Photobiol. A; Chem., 157 (2003) 103–109.

[23] K.H. Choo, D.I. Chang, K.W. Park and M.H. Kim, Use of an integrated photocatalysis/hollow fiber microfiltration system for the removal of trichloroethylene in water, J. Haz. Mat., 152 (2008) 183–190.

[24] J. Orantes, C. Wisniewski, M. Heran and A. Grasmick, The influence of operating conditions on permeability changes in a submerged membrane bioreactor, Sep. Purif. Technol., 52 (2006) 60–66.

[25] T.E. Doll and F.H. Frimmel, Cross-flow microfiltration with periodical back-washing for photocatalytic degradation of pharmaceutical and diagnostic residues—evaluation of the long term stability of the photocatalytic activity of TiO_2, Water Res., 39 (2005) 847–854.

[26] J. Fu, M. Ji, Z. Wang, L. Jin and D. An, A new submerged membrane photocatalytic reactor (SMPR) for fulvic acid removal using a nano-stuctured photocatalyst, J. Haz. Mat., B131 (2006) 238–242.